

Probing the Primordial Power Spectrum with Cluster Number Counts

Teeraparb Chantavat^{1*}, Christopher Gordon^{1†}, Joseph Silk^{1‡}

¹*Department of Astrophysics, University of Oxford, Keble Road, OX1 3RH, UK.*

ABSTRACT

We investigate how well galaxy cluster number counts can constrain the primordial power spectrum. Measurements of the primary anisotropies in the cosmic microwave background (CMB) may be limited, by the presence of foregrounds from secondary sources, to probing the primordial power spectrum at wave numbers less than about $0.2 h\text{Mpc}^{-1}$. We find that cluster number counts could then play a valuable role in tightly constraining the form of the primordial power spectrum up to wave numbers of about $0.3 h\text{Mpc}^{-1}$. We provide forecasts for constraints on the primordial power spectrum for combinations of the PLANCK and the South Pole Telescope primary anisotropy CMB data and their Sunyaev-Zel’dovich effect derived cluster samples.

Key words:

1 INTRODUCTION

A crucial element of cosmology is the form of the primordial fluctuations. These fluctuations provide the seeds for structure formation which we observe today through the cosmic microwave background (CMB), galaxy, and cluster surveys. Current data is consistent with the primordial fluctuations being scalar, adiabatic, Gaussian and having a power spectrum with a simple power law parameterization (Spergel 2007; Komatsu et al. 2008). The primordial fluctuations may have been generated during a period, known as ‘inflation’, of accelerated expansion of the primordial Universe driven by a potential dominated scalar field or fields (see for example Liddle & Lyth (2000)). If inflation was driven by a single scalar field with a smooth potential, then the power spectrum of primordial fluctuation is predicted to be generally quite close to a power law form, although in some cases there may be significant running of the spectral index. However, if inflation was driven by multiple fields or by a single field with a feature in its potential, then the primordial power spectrum may contain hills, valleys, oscillations or other features (see for example Salopek et al. (1989); Leach et al. (2001); Joy et al. (2008); Enea Romano & Sasaki (2008)).

The two main approaches to probing the primordial power spectrum are either to assume a specific form for a feature in the primordial power spectrum (see for example Bond (1988); Hamann et al. (2007); Hoi et al. (2007); Joy et al. (2008)) or to try and reconstruct the primor-

dial power spectrum non-parametrically (see for example Bridle et al. (2003); Hu & Okamoto (2004); Leach (2006); Zhan et al. (2006); Spergel (2007); Shafieloo & Souradeep (2008); Verde & Peiris (2008)). The cleanest probe of the primordial power-spectrum is the cosmic microwave background (CMB). However, it is probably limited to wave numbers smaller than about $0.2 h\text{Mpc}^{-1}$ as beyond that foreground contamination from secondary sources are likely to dominate the cosmological signal.

In this article, we investigate to what extent galaxy cluster number counts can probe the primordial power spectrum. We begin in Section 2 with contrasting how the cluster number counts and the primary CMB probe the primordial power spectrum. In Section 3 we forecast the constraints on the primordial power spectrum from the Sunyaev-Zeldovich effect (SZ) PLANCK¹ and South Pole Telescope² (SPT) cluster surveys and combine them with the forecasted constraints on the primordial power spectrum from the PLANCK and SPT primary CMB survey. Concluding remarks are given in Section 4.

2 DEPENDENCE ON PRIMORDIAL POWER SPECTRUM

The dimensionless primordial power spectrum, as function of the comoving wave number k , is usually parameterized as a power law

* Email:txc@astro.ox.ac.uk

† Email:cxg@astro.ox.ac.uk

‡ Email:silk@astro.ox.ac.uk

¹ <http://www.rssd.esa.int/index.php?project=planck>

² <http://pole.uchicago.edu/>

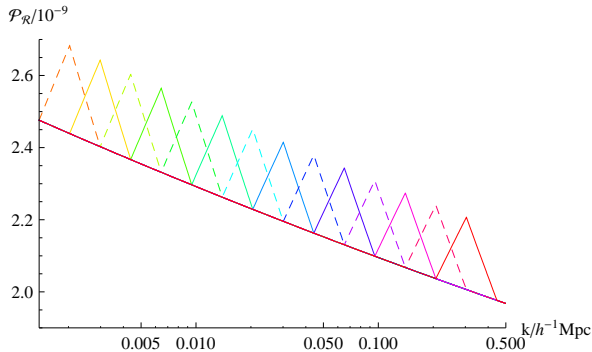


Figure 1. The effect on the primordial power spectrum of individually changing nodes 1 to 14 to 1.1 in our feature function F . Each changed node is plotted as a separate colour and odd numbered nodes are plotted as dashed lines.

$$\mathcal{P}_{\mathcal{R},0}(k) \equiv \Delta_{\mathcal{R}}^2 \left(\frac{k}{k_{\text{pivot}}} \right)^{n-1} \quad (1)$$

where the amplitude ($\Delta_{\mathcal{R}}^2$), spectral index (n), and pivot point (k_{pivot}) are taken to be independent of k . We model deviations from this form in a similar way to Bridle et al. (2003); Spergel (2007):

$$\mathcal{P}_{\mathcal{R}}(k) = F(k) \mathcal{P}_{\mathcal{R},0}(k) \quad (2)$$

where the “feature function”, $F(k)$, is specified by the values at 16 nodes logarithmically spaced in k -space with

$$\frac{k_i}{h^{-1}\text{Mpc}} = \frac{0.447}{1.47^i}, \quad i = 0, \dots, 15. \quad (3)$$

Linear interpolation in $\log(k)$ is used to determine F between each node. The effect of individually changing nodes 1 to 14 is shown in Fig. 1. Nodes 0 and 15 will always be fixed to 1.

2.1 Effect on number counts

The linear theory matter power spectrum at a redshift z is given by

$$P(k, z) = T^2(k, z) \frac{2\pi^2}{k^3} \mathcal{P}_{\mathcal{R}}(k) \quad (4)$$

where T is the matter transfer function. We use CAMB³ (Lewis et al. 2000) to evaluate P and we modified the “ScalarPower” function in CAMB to include our feature function F . The accuracy and sample boost parameters in the CAMB initialization file were all set to the value of 3 which increases the precision and reduces the amount of interpolation. Although, there is some interpolation in k used by CAMB, the sampling is much smaller than the width between our nodes. Throughout this paper we assume a flat Λ CDM Universe with no tensor perturbations and we use the WMAP5 maximum likelihood parameters (Dunkley & Others 2008):

$$\Omega_b h^2 = 0.0227, \quad \Omega_c h^2 = 0.108, \quad n = 0.961, \quad \tau = 0.089, \\ \Delta_{\mathcal{R}}^2 = 2.41 \times (500/20)^{0.961-1} \times 10^{-9}, \quad h = 0.724, \quad (5)$$

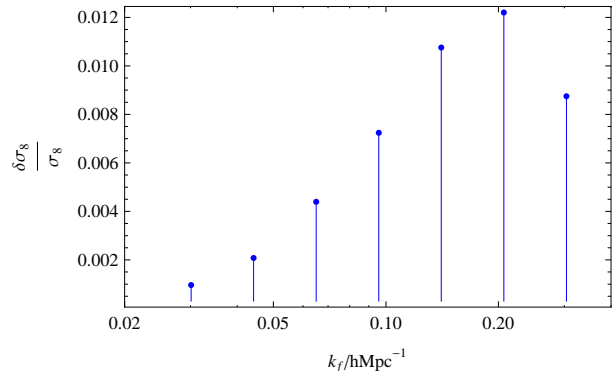


Figure 2. Effect of individually setting the node at $F[k_f] = 1.1$ on the variance of the matter field smoothed with $8h^{-1}\text{Mpc}$ top hat window function.

where we have converted the primordial power spectrum amplitude to correspond to the default CAMB pivot of $k_{\text{pivot}} = (1/20)\text{Mpc}^{-1}$.

The variance of the linear theory matter field, which has been smoothed by a top hat filter on a comoving length scale R , is given by

$$\sigma^2(R, z) = \int_0^\infty \frac{dk}{k} \frac{k^3}{2\pi^2} P(k, z) W^2(kR) \quad (6)$$

where

$$W(kR) = 3 \left[\frac{\sin(kR)}{(kR)^3} - \frac{\cos(kR)}{(kR)^2} \right]. \quad (7)$$

The top hat smoothing suppresses the contribution of any fluctuations located at wave number $k_f \gg 1/R$. Fig. 2 illustrates how changing the primordial power spectrum effects σ .

For a background non-relativistic matter density of $\rho_m = \Omega_m \rho_{\text{total}}$, the number density (n) of halos (bound objects) of mass

$$M = \frac{4\pi}{3} R^3 \rho_m = 1.16 \times 10^{12} \Omega_m h^{-1} \left(\frac{R}{h^{-1}\text{Mpc}} \right)^3 M_\odot \quad (8)$$

depends, to a good approximation, on the primordial power spectrum only through its effect on $\sigma(R, z)$ (Press & Schechter 1974; Sheth & Tormen 1999; Sheth et al. 2001; Knebe et al. 2001; Jenkins et al. 2001)

$$\frac{dn(z)}{dM} = \frac{\rho_m}{M} \frac{d \ln \sigma(z)^{-1}}{dM} f(\sigma(z)). \quad (9)$$

We use the Sheth-Tormen mass function which takes into account the ellipsoidal nature of halo formation (Sheth & Tormen 1999; Sheth et al. 2001) and for which

$$f = A \sqrt{\frac{2a}{\pi}} \left[1 + \left(\frac{\sigma(z)^2}{a \delta_c^2} \right)^p \right] \frac{\delta_c}{\sigma(z)} \exp \left(-\frac{a \delta_c^2}{2 \sigma(z)^2} \right) \quad (10)$$

where $A = 0.3222$, $a = 0.707$, $p = 0.3$, and $\delta_c = 1.686$. The top hat smoothing in Eq. (6) suppresses the contribution of any change to the primordial power spectrum located at wave number $k_f \gg 1/R$. Combined with Eq. (8), this implies that a change in the primordial power spectrum at k_f has a suppressed effect on the number density on mass scales satisfying

³ <http://camb.info/>

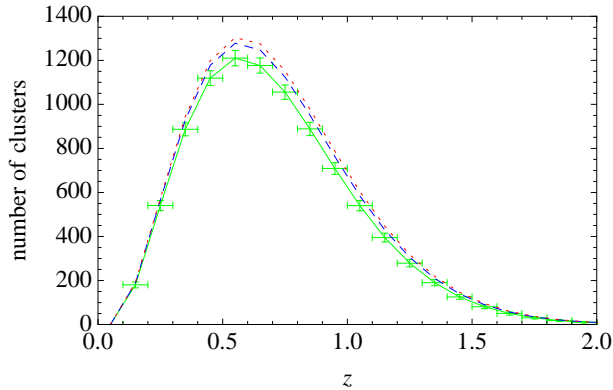


Figure 3. Effect of change in primordial power spectrum on SPT. The plots are for the featureless ($F = 1$) power spectrum (green, solid), $F[0.30] = 1.1$ (blue dashed), and $F[0.21] = 1.1$ (red dotted).

$$\frac{M}{h^{-1}M_{\odot}} \gg 10^{12} \left(\frac{k_f}{h\text{Mpc}^{-1}} \right)^{-3}. \quad (11)$$

The number of clusters per redshift interval above some mass threshold M_{\min} is given by

$$\frac{dN}{dz}(M > M_{\min}) = f_{\text{sky}} \frac{dV(z)}{dz} \int_{M_{\min}}^{\infty} dM \frac{dn}{dM}(M, z). \quad (12)$$

Where f_{sky} is the fraction of the sky being observed and the volume element is given by

$$\frac{dV}{dz} = \frac{4\pi}{H(z)} \left[\int_0^z \frac{dz'}{H(z')} \right]^2 \quad (13)$$

and $H(z)$ is the Hubble parameter

$$H(z) = H_0 \sqrt{(\Omega_m(1+z)^3 + (1 - \Omega_m))}. \quad (14)$$

The effect of a change in the primordial power spectrum on the number counts is illustrated in Fig. 3 for the South Pole Telescope (SPT) (Ruhl & Others 2004) (see Sec. 3). We approximate the SPT selection function by setting $M_{\min} = 1.75 \times 10^{14} h^{-1} M_{\odot}$ in Eq. (12). Due to the exponential suppression in Eq. (10), dN/dz mainly depends on the mass scale M_{\min} . From Eq. (11) this implies SPT will become insensitive to the primordial power spectrum for $k \gg 0.2$. This is consistent with $F[0.30] = 1.1$ having less of an effect than $F[0.21] = 1.1$ as illustrated in Fig. 3. Note however how the shape of the effect of changing $F[0.30]$ and $F[0.21] = 1.1$ is very similar. This means that a positive value in the former node can be almost completely cancelled by the latter. This is an illustration of how the cluster number counts are good at constraining the amplitude of a feature in the primordial power spectrum but only if the location is fixed by some other method.

2.2 Effect on the CMB

The primordial power spectrum is probed over a wide range of wave numbers by measurements of the primary CMB anisotropies (see for example Hu & Okamoto (2004)). Both the temperature (T) and E-mode of the polarization (E) probe scalar perturbations. Lensing of the E-mode can generate B-modes of polarization which may contain useful

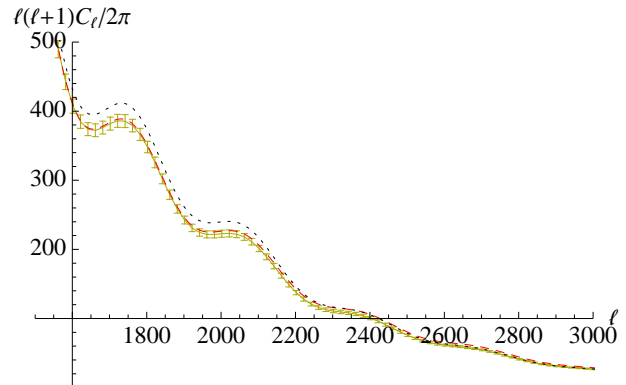


Figure 4. Effect of change in primordial power spectrum on the CMB (TT). Error bars (plotted at each 20th ℓ for clarity) centered on the featureless ($F = 1$) (yellow) power spectrum are for SPT. The $F[0.30] = 1.1$ (red dashed), and $F[0.21] = 1.1$ (black dotted) are also plotted. Perfect subtraction of secondary foreground sources is assumed for the figure

cosmological information (Smith et al. 2004; Hu et al. 2006; Smith et al. 2006) and could possibly also be useful in probing the primordial power spectrum. However, their inclusion is beyond the scope of the present paper. The angular power spectrum of the CMB is given by a transfer function weighted integral of the primordial power spectrum

$$\frac{\ell(\ell+1)C_{\ell}^{XX'}}{2\pi} = \int d \ln k T_{\ell}^X(k) T_{\ell}^{X'}(k) \mathcal{P}_{\mathcal{R}}(k) \quad (15)$$

where $X, X' \in T, E$. The projection of a mode of wave-number k on to the surface of last scattering (a sphere of comoving radius D_*) results in the CMB transfer functions having the form $T_{\ell}^X \sim j_{\ell}(kD_*)$. Where j_{ℓ} is the spherical Bessel function of order ℓ which peaks at $\ell \approx kD_*$. Therefore a feature in the primordial power spectrum at wave-number k_f is mapped onto a feature in CMB angular power spectrum at

$$\ell \sim k_f D_* \approx 10^4 \frac{k_f}{h\text{Mpc}^{-1}} \quad (16)$$

We also used our modified version of CAMB to evaluate $C_{\ell}^{XX'}$. Although, there is some interpolation in ℓ used by CAMB, the sampling is much smaller than the width between our nodes. Fig. 4 shows the effect $F \neq 1$ on C_{ℓ}^{TT} with predicted SPT error bars (see Sec. 3). In the figure we have not included the foreground contribution from secondary sources which will probably be hard to completely remove for $\ell > 2000$. For this reason, as in (Hu & Okamoto 2004; Leach 2006), we will restrict ourselves to $\ell \leq 2000$ when evaluating the forecasted marginalized errors.

3 FORECASTS

We use the Fisher matrix formalism to make forecasts on how well the primordial power spectrum can be constrained. We take as our fiducial model the WMAP5 maximum likelihood parameters, Eq. (5). We consider two cluster count SZ experiments: PLANCK and SPT. For PLANCK we take $f_{\text{sky}} = 0.8$ and $M_{\min} = 5 \times 10^{14} h^{-1} M_{\odot}$ (Geisbüsich & Hobson 2007). For SPT we take $f_{\text{sky}} = 0.1$

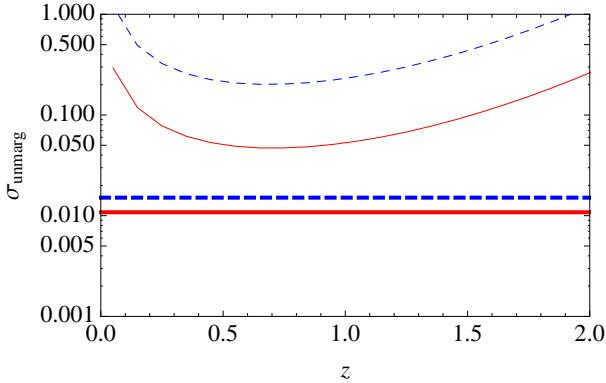


Figure 5. A plot of the expected one standard deviation error for SPT as a function of the center of a red shift bin of width 0.1. The $F[0.30] = 1.1$ (blue dashed), and $F[0.21] = 1.1$ (red solid) are plotted. The thick horizontal lines are the corresponding expected one standard deviation error when all the redshift bins from 0 to 3 are combined.

and $M_{\min} = 1.75 \times 10^{14} h^{-1} M_{\odot}$. We take $z \in [0, 3]$ with bin sizes $\delta z = 0.1$, although the bulk of the constraining power comes from $z < 1$. The number of clusters in redshift bin i is Poisson distributed with the expected number (e_i) given by integrating Eq. (12) over the red shift bin. Element (j, k) of the Fisher matrix for a cluster count experiment is given by (Holder et al. 2001)

$$\mathcal{F}_{jk} = \sum_{i=1}^{N_{\text{bins}}} \frac{1}{e_i} \frac{\partial e_i}{\partial p_j} \frac{\partial e_i}{\partial p_k} \quad (17)$$

where p_j consists of the cosmological parameters in Eq. (5) except for $\Delta_{\mathcal{R}}^2$ and n as they will be almost completely degenerate with the feature function F . To account for uncertainties in the mass of the observed clusters, we also allow M_{\min} to be a free parameter. Additionally, we allow the nodes 1 to 14 in Eq. (3) of F to vary. The derivatives are taken at the fiducial values of the parameters which in the case of M_{\min} is the actual minimum mass cluster observable by the experiment and $F(k_i) = 1$ for all i . The derivatives are approximated by the symmetrized form of a difference equation so as to minimize truncation error (see for example Press et al. (1992)). A step of 2.5% each side of the fiducial value was used.

The expected one standard deviation unmarginalized error of parameter p_i can be approximated by $1/\sqrt{F_{ii}}$. The forecasted SPT value is plotted for each individual red shift bin for a couple of example cases in Fig. 5. As can be seen, the clusters at $z \sim 0.5$ provided the tightest constraints. This is because that is where the number of detected clusters (and hence signal to noise ratio) is maximized.

The CMB Fisher matrix is given by (see for example (Zaldarriaga et al. 1997))

$$\mathcal{F}_{ij} = \sum_{\ell} \sum_{X, X'} \frac{\partial C_{\ell}^X}{\partial p_i} \text{Cov}^{-1}(C_{\ell}^X, C_{\ell}^{X'}) \frac{\partial C_{\ell}^{X'}}{\partial p_j} \quad (18)$$

where the covariance matrix can be obtained in (Zaldarriaga et al. 1997) and it depends on the temperature noise per pixel (σ_T), the polarization noise per pixel (σ_E), the pixel area in radians squared ($\theta^2 = 4\pi/N_{\text{pix}}$), and the beam window function which we approximate as

Table 1. PLANCK Instrument Characteristics

Center Frequency (GHz)	70	100	143	217
θ (FWHM arcmin)	14	10	7.1	5.0
σ_T (μK)	12.8	6.8	6.0	13.1
σ_E (μK)	18.2	10.9	11.4	26.7

Gaussian ($B_{\ell} \approx \exp(-\ell(\ell+1)\sigma_b^2)$). The values we use are taken from the PLANCK blue book⁴ and are listed in Table 1 (note that θ needs to be converted to radians). We use $\sigma_b = \theta/\sqrt{8 \log[2]}$ and combine the different frequency bands as specified in Bond et al. (1997). We also include the constraints from SPT primary CMB temperature measurement for which we just use one band with $\theta = 1$ arcmin and $\sigma_T = 10 \mu\text{K}$. We take the range in ℓ to be 2 to 2000. At higher ℓ , secondary sources of temperature and polarization will likely prohibit the extraction of cosmological information from the primary CMB.

Some examples of the unmarginalized errors for each ℓ -mode are plotted in Fig. 6. As can be seen, PLANCK (TT,TE,EE) provides a better constraint than SPT (TT) except at the higher ℓ values where the smaller beam size of SPT gives it an advantage. The figure assumes perfect removal of secondary sources which will be very challenging for $\ell > 2000$. But, as can be seen in Fig. 6, the $F[0.30]$ node is not well constrained by the primary CMB for our assumed constraint of $\ell \leq 2000$.

The expected covariance matrix of the parameter errors is approximated by the inverse of the Fisher matrix. The expected marginalized one sigma error bars are then given by the square roots of the diagonal elements of the expected covariance matrix. Also, experiments can be combined by adding the Fisher matrices. When we combine PLANCK and SPT, primary CMB or SZ cluster detection, we reduce the f_{sky} for PLANCK to 0.7. We plot the expected one sigma marginalized errors for F in Fig. 7. The lack of constraint at low k is from cosmic variance. At high k , the primary CMB does not constrain the primordial power spectrum as it is limited to $\ell \leq 2000$ due to secondary sources. As shown in Fig. 7, including the SPT clusters makes a big improvement in constraining the primordial power spectrum at $k = 0.30 h \text{Mpc}^{-1}$.

The marginalized one sigma errors for the cosmological parameters and the last two variable nodes of F are presented in Table 2. One notable feature of Table 2 is how dramatically the error in the cosmological parameters is decreased in the last row. This is due to breaking of degeneracies when the primary CMB and clusters are combined as illustrated in Fig. 8. The higher mass minimum mass threshold of the PLANCK cluster survey means it detects less clusters and so has a higher Poisson noise than the SPT cluster survey. Adding it to the experiments in the final row of Table 2 has little effect. But the primary CMB measurement from PLANCK is still needed to constrain the cosmological parameters and the primordial power spectrum at $k \leq 0.2 h \text{Mpc}^{-1}$.

⁴ [http://www.rssd.esa.int/SA/PLANCK/docs/Bluebook-ESA-SCI\(2005\)1_LV2.pdf](http://www.rssd.esa.int/SA/PLANCK/docs/Bluebook-ESA-SCI(2005)1_LV2.pdf)

Table 2. Expected marginalized one sigma errors for the feature function (F) and the cosmological parameters. The other nodes of F and M_{\min} where also allowed to vary.

Observations	h	$\Omega_c h^2$	$\Omega_b h^2$	τ	$F(0.21)$	$F(0.30)$
PLANCK (TT, TE, EE)	0.0073	0.0014	0.0002	0.0045	0.0151	0.1020
PLANCK (TT, TE, EE, Clusters)	0.0072	0.0014	0.0002	0.0024	0.0146	0.0916
PLANCK (TT, TE, EE), & SPT (TT)	0.0076	0.0015	0.0002	0.0048	0.0137	0.0737
PLANCK (TT, TE, EE) & SPT (TT, Clusters)	0.0006	0.0002	0.0001	0.0015	0.0077	0.0228

4 CONCLUSIONS

In this article we have investigated what role cluster number counts can play in constraining the primordial power spectrum. We found that they provide a large improvement at around $k = 0.30 h\text{Mpc}^{-1}$ if the usable primary CMB is limited to $\ell \leq 2000$ by secondary source foregrounds. In particular we found that the combination of the PLANCK and SPT primary CMB observations with the SPT cluster number counts will provide tight constraints on the primordial power spectrum up to $k = 0.30 h\text{Mpc}^{-1}$ and also dramatically increase the precision on the other cosmological parameters compared to just using the primary CMB alone.

It would be interesting to repeat the investigation here with a more realistic selection function for the SPT SZ cluster survey. Another interesting extension would be to evaluate the possible constraints from Atacama Cosmology Telescope (ACT) (Kosowsky 2003) and future X-RAY cluster surveys such as the XMM wide survey (Pierre et al. 2008).

5 ACKNOWLEDGEMENT

We thank Dick Bond, Joe Dunkley, Sam Leach, Anze Slosar, and Joe Zuntz for helpful discussions. TC is funded by The Institute for the Promotion of Teaching and Science and Technology (IPST) in Thailand. CG is funded by the Beecroft Institute for Particle Astrophysics and Cosmology.

REFERENCES

- Bond J. R., 1988, Probing cosmic density fluctuation spectra. Large-Scale Motions in the Universe: A Vatican study Week, pp 419–435, ADS
- Bond J. R., Efstathiou G., Tegmark M., 1997, MNRAS, 291, L33, ADS, arXiv:astro-ph/9702100
- Bridle S. L., Lewis A. M., Weller J., Efstathiou G., 2003, MNRAS, 342, L72, ADS, arXiv:astro-ph/0302306
- Dunkley J., Others 2008, 0803.0586
- Enea Romano A., Sasaki M., 2008, ArXiv e-prints, ADS, 0809.5142
- Geisbüsch J., Hobson M. P., 2007, MNRAS, 382, 158, ADS, arXiv:astro-ph/0611567
- Hamann J., Covi L., Melchiorri A., Slosar A., 2007, Phys. Rev. D, 76, 023503, ADS, arXiv:astro-ph/0701380
- Hoi L., Cline J. M., Holder G. P., 2007, ArXiv e-prints, ADS, 0706.3887
- Holder G., Haiman Z., Mohr J. J., 2001, ApJ, 560, L111, ADS, arXiv:astro-ph/0105396
- Hu W., Huterer D., Smith K. M., 2006, ApJ, 650, L13, ADS, arXiv:astro-ph/0607316
- Hu W., Okamoto T., 2004, Phys. Rev. D, 69, 043004, ADS, arXiv:astro-ph/0308049
- Jenkins A., Frenk C. S., White S. D. M., Colberg J. M., Cole S., Evrard A. E., Couchman H. M. P., Yoshida N., 2001, MNRAS, 321, 372, ADS, arXiv:astro-ph/0005260
- Joy M., Shafieloo A., Sahni V., Starobinsky A. A., 2008, ArXiv e-prints, ADS, 0807.3334
- Knebe A., Islam R. R., Silk J., 2001, MNRAS, 326, 109, ADS, arXiv:astro-ph/0103082
- Komatsu E., Dunkley J., Nolta M. R., Bennett C. L., Gold B., Hinshaw G., Jarosik N., Larson D., Limon M., Page L., Spergel D. N., Halpern M., Hill R. S., Kogut A., Meyer S. S., Tucker G. S., Weiland J. L., Wollack E., Wright E. L., 2008, ArXiv e-prints, ADS, 0803.0547
- Kosowsky A., 2003, New Astronomy Review, 47, 939, ADS, arXiv:astro-ph/0402234
- Leach S., 2006, MNRAS, 372, 646, ADS, arXiv:astro-ph/0506390
- Leach S. M., Sasaki M., Wands D., Liddle A. R., 2001, Phys. Rev. D, 64, 023512, ADS, arXiv:astro-ph/0101406
- Lewis A., Challinor A., Lasenby A., 2000, ApJ, 538, 473, astro-ph/9911177
- Liddle A. R., Lyth D. H., 2000, Cosmological Inflation and Large-Scale Structure. Cosmological Inflation and Large-Scale Structure, by Andrew R. Liddle and David H. Lyth, pp. 414. ISBN 052166022X. Cambridge, UK: Cambridge University Press, April 2000., ADS
- Pierre M., Pacaud F., Melin J. B., consortium X.-L., 2008, Astronomische Nachrichten, 329, 143, ADS, 0712.0262
- Press W. H., Schechter P., 1974, ApJ, 187, 425, ADS
- Press W. H., Teukolsky S. A., Vetterling W. T., Flannery B. P., 1992, Numerical recipes in FORTRAN. The art of scientific computing. Cambridge: University Press, —c1992, 2nd ed., ADS
- Ruhl J., Others 2004, in Bradford C. M., Ade P. A. R., Aguirre J. E., Bock J. J., Dragovan M., Duband L., Earle L., Glenn J., Matsuhara H., Naylor B. J., Nguyen H. T., Yun M., Zmuidzinas J., eds, Society of Photo-Optical Instrumentation Engineers (SPIE) Conference Series Vol. 5498 of Society of Photo-Optical Instrumentation Engineers (SPIE) Conference Series, The South Pole Telescope. pp 11–29, ADS
- Salopek D. S., Bond J. R., Bardeen J. M., 1989, Phys. Rev. D, 40, 1753, ADS
- Shafieloo A., Souradeep T., 2008, Phys. Rev. D, 78, 023511, ADS, 0709.1944
- Sheth R. K., Mo H. J., Tormen G., 2001, MNRAS, 323, 1,

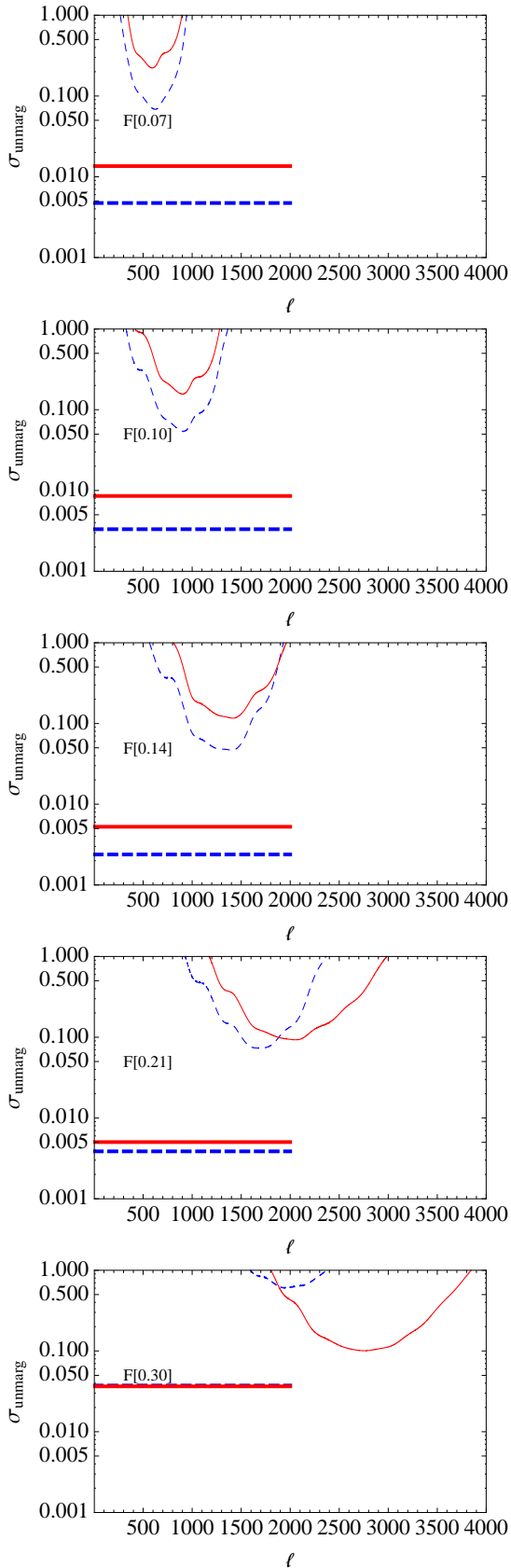


Figure 6. The unmarginalized one sigma errors from PLANCK (TT,EE,TE) (red,solid) and SPT (TT) (blue dashed) for the individual ℓ modes. In each panel the error is for the F at the specified node, where the argument is the wave number in units of $h\text{Mpc}^{-1}$. The horizontal line is for the overall unmarginalized

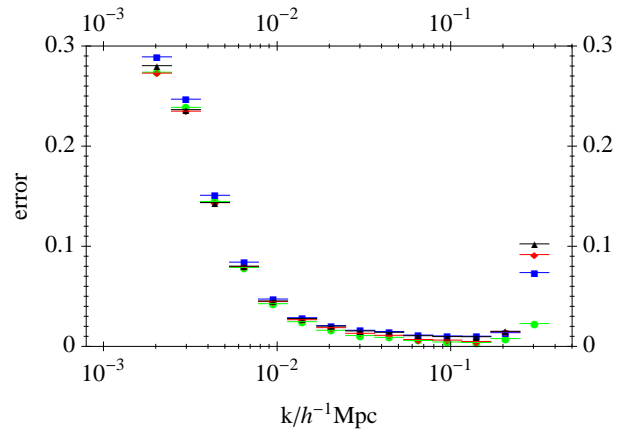


Figure 7. Expected marginalized one sigma errors for the feature function (F). Errors are shown for PLANCK (TT, TE, EE) (black triangles), PLANCK (TT, TE, EE, clusters) (red diamonds), PLANCK (TT,TE,EE) and SPT (TT) (blue squares), and PLANCK (TT, TE, EE) and SPT (TT, clusters) (green circles)

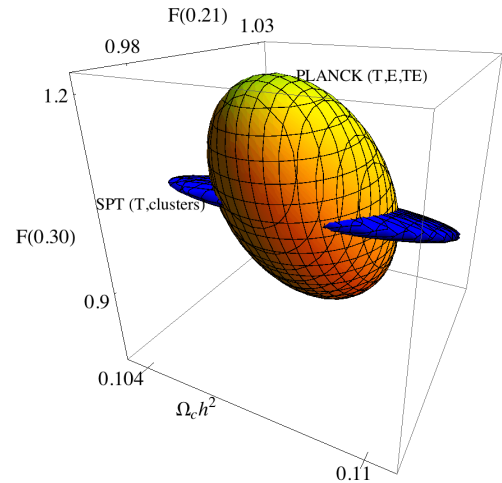


Figure 8. Marginalized ellipsoids containing 68% of the expected posterior probability. The arguments for the feature function F are in $h\text{Mpc}^{-1}$.

- ADS, arXiv:astro-ph/9907024
 Sheth R. K., Tormen G., 1999, MNRAS, 308, 119, ADS, arXiv:astro-ph/9901122
 Smith K. M., Hu W., Kaplinghat M., 2004, Phys. Rev. D, 70, 043002, ADS, arXiv:astro-ph/0402442
 Smith K. M., Hu W., Kaplinghat M., 2006, Phys. Rev. D, 74, 123002, ADS, arXiv:astro-ph/0607315
 Spergel D. N. o., 2007, Astrophys. J. S., 170, 377, ADS, arXiv:astro-ph/0603449
 Verde L., Peiris H., 2008, Journal of Cosmology and Astro-Particle Physics, 7, 9, ADS, 0802.1219
 Zaldarriaga M., Spergel D. N., Seljak U., 1997, ApJ, 488, 1, ADS, arXiv:astro-ph/9702157
 Zhan H., Knox L., Tyson J. A., Margoniner V., 2006, ApJ, 640, 8, ADS, arXiv:astro-ph/0508119